Electronic Supplementary Information

An Enhanced Electrochemical CO_2 Reduction Reaction on the SnOx-PdO surface of SnPd Nanoparticles Decorated on N-doped Carbon Fibers

Sreekanth Narayanaru[a,b], Gopinathan M Anilkumar[a,b,c], Masaki ito[c], Takanori Tamaki[a,b], and Takeo Yamaguchi[a,b*]

[a] Laboratory for Chemistry and Life Sciences,
Tokyo Institute of Technology, R1-17, 4259 Nagatsuta, Midori-Ku, Yokohama 226-850
[b] Core Research for Evolutionary Science and Technology, Japan Science and Technology Agency
(JST-CREST), Japan 102-0076

[c] R&D Centre, Noritake Co., Ltd, 300 Higashiyama, Miyochi-cho, Miyoshi, Japan 470-0293

*E-mail: yamag@res.titech.ac.jp

S1. ICP Data

Catalyst	Total amount of catalyst (including NCF) (mg)	Weight of the metal present in 10 mg of sample (mg) Sn	Pd	Wt.% of Sn in total metal loading $\left[\frac{Sn}{Sn+Pd}\right]*100$	Wt.% of Pd in total metal loading $\left[\frac{Pd}{Sn+Pd}\right]*100$
Sn_{100}-NCF	10	3.63	0	100	
$Sn_{97}Pd_3$-NCF	10	2.67	0.08	97.01	2.99
$Sn_{95}Pd_5$-NCF	10	3.70	0.19	95.02	4.98
$Sn_{94}Pd_6$-NCF	10	3.75	0.22	94.33	5.67
$Sn_{91}Pd_9$-NCF	10	4.16	0.39	91.33	8.67

Table S1. The weight distribution of individual metals present in Sn100–NCF and $Sn_{100-y}Pd_y$–NCF

S2. XPS Analysis

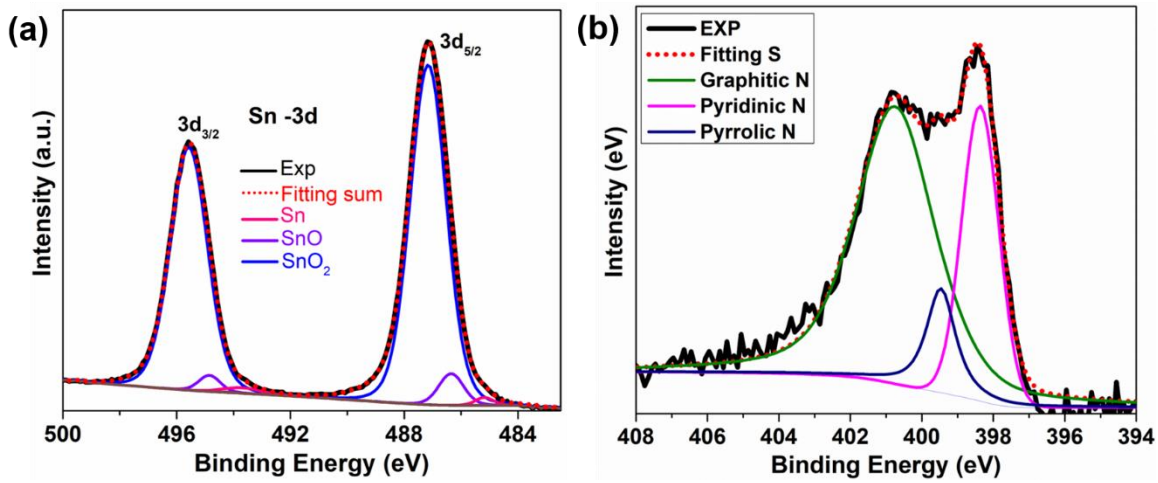

Figure S1. XPS spectra of Sn_{100}–NCF. De-convoluted spectra of (a) Sn and (b) N.

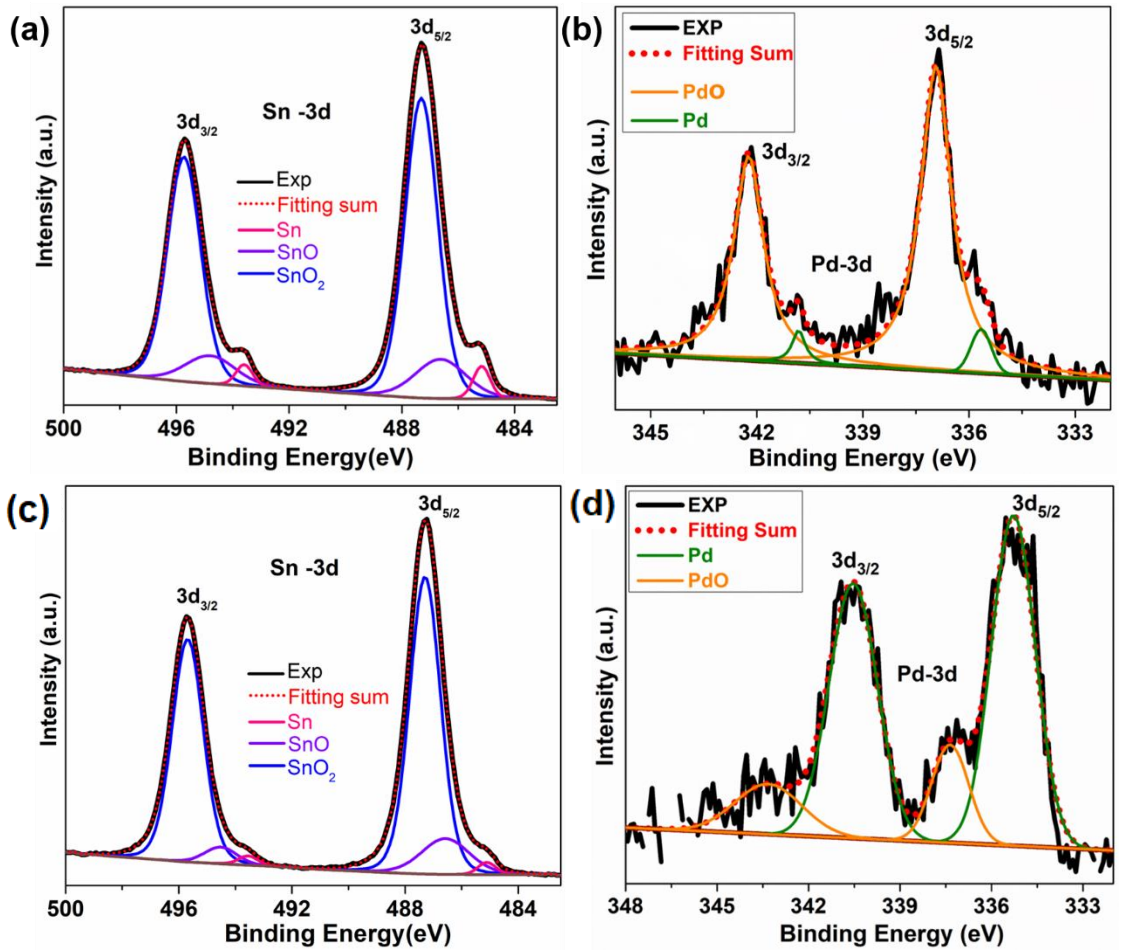

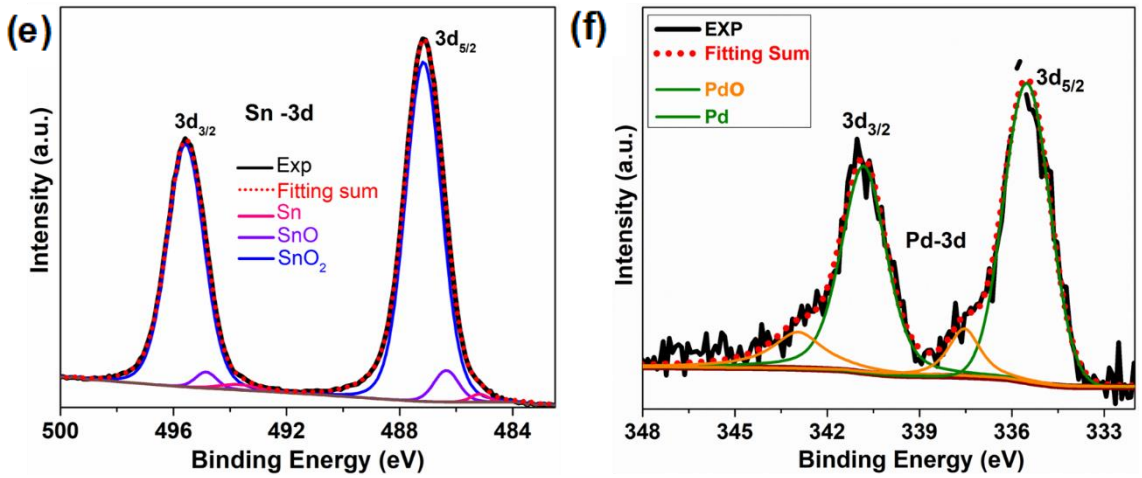

Figure S2. Deconvoluted XPS Sn and Pd spectra of (a) & (b) $Sn_{95}Pd_5$–NCF, (c) & (d) $Sn_{94}Pd_6$–NCF and (e) & (f) $Sn_{91}Pd_9$–NCF.

S2.1 Calculation of the atomic percentage from XPS data

The atomic percentage of each oxidation state of Sn and Pd present in a catalyst was calculated from its corresponding deconvoluted XPS spectrum. The percentages of different oxidation states of Sn were calculated by measuring the peak area of Sn, SnO and SnO_2 in the deconvoluted Sn -$3d_{5/2}$ peak, and then the area of a particular oxidation state was divided by the total area of the peak and then multiplied by 100 to obtain the percentage.

The area under the curve of Sn, SnO^{2+}, and SnO_2 in the Sn -$3d_{5/2}$ peak is defined as A_{Sn}, $A_{SnO,}$ and A_{SnO2}, respectively.

The total area of the Sn -$3d_{5/2}$ peak was calculated as $A_{Sn\ -3d5/2} = A_{Sn} + A_{SnO} + A_{SnO2}$.

The percentage of Sn in the Sn -$3d_{5/2}$ peak was calculated as % Sn = $(A_{Sn0}/A_{Sn\ -3d5/2})$ x100.

Similarly, we calculated the atomic percentage of the different oxidation states of Pd, *i.e.*, Pd and PdO, from the deconvoluted Pd-$3d_{5/2}$ peak.

(a)

Catalyst	Sn ($3d_{5/2}$)			SnO ($3d_{5/2}$)			SnO_2 ($3d_{5/2}$)		
	Position (eV)	Peak Area	Atomic %	Position (eV)	Peak Area	Atomic %	Position	Peak Area	Atomic %
Sn_{100}–NCF	485.17	121.8	1.07	486.28	674.2	5.93	487.25	10556.4	93.0
$Sn_{97}Pd_3$–NCF	485.18	810.6	3.26	486.28	3263.2	13.14	487.31	20744.9	83.60
$Sn_{95}Pd_5$–NCF	485.17	376.2	1.88	486.26	1053.5	5.26	487.30	18593.1	92.86
$Sn_{94}Pd_6$–NCF	485.15	229.3	1.93	486.32	1821.0	15.44	487.29	9749.3	82.63
$Sn_{91}Pd_9$–NCF	485.19	635.6	2.75	486.23	1033.7	4.46	487.26	21478.4	92.79

(b)

Catalyst	Pd ($3d_{5/2}$)			PdO ($3d_{5/2}$)		
	Position (eV)	Peak Area	Atomic %	Position (eV)	Peak Area	Atomic %
$Sn_{97}Pd_3$–NCF				336.9	230.8	100
$Sn_{95}Pd_5$–NCF	335.5	20.6	5.86	336.9	330.8	94.14
$Sn_{94}Pd_6$–NCF	336.2	342.3	80.80	337.3	81.3	19.20
$Sn_{91}Pd_9$–NCF	336.4	566.4	91.59	337.5	52.0	8.41

Table S2. XPS peak position, peak area, and atomic percentage of (a) Sn, SnO, SnO_2, (b) Pd and PdO in various SnPd-NCF catalysts.

S3. EDS Analysis of the Elemental Composition of SnPd–NCFs

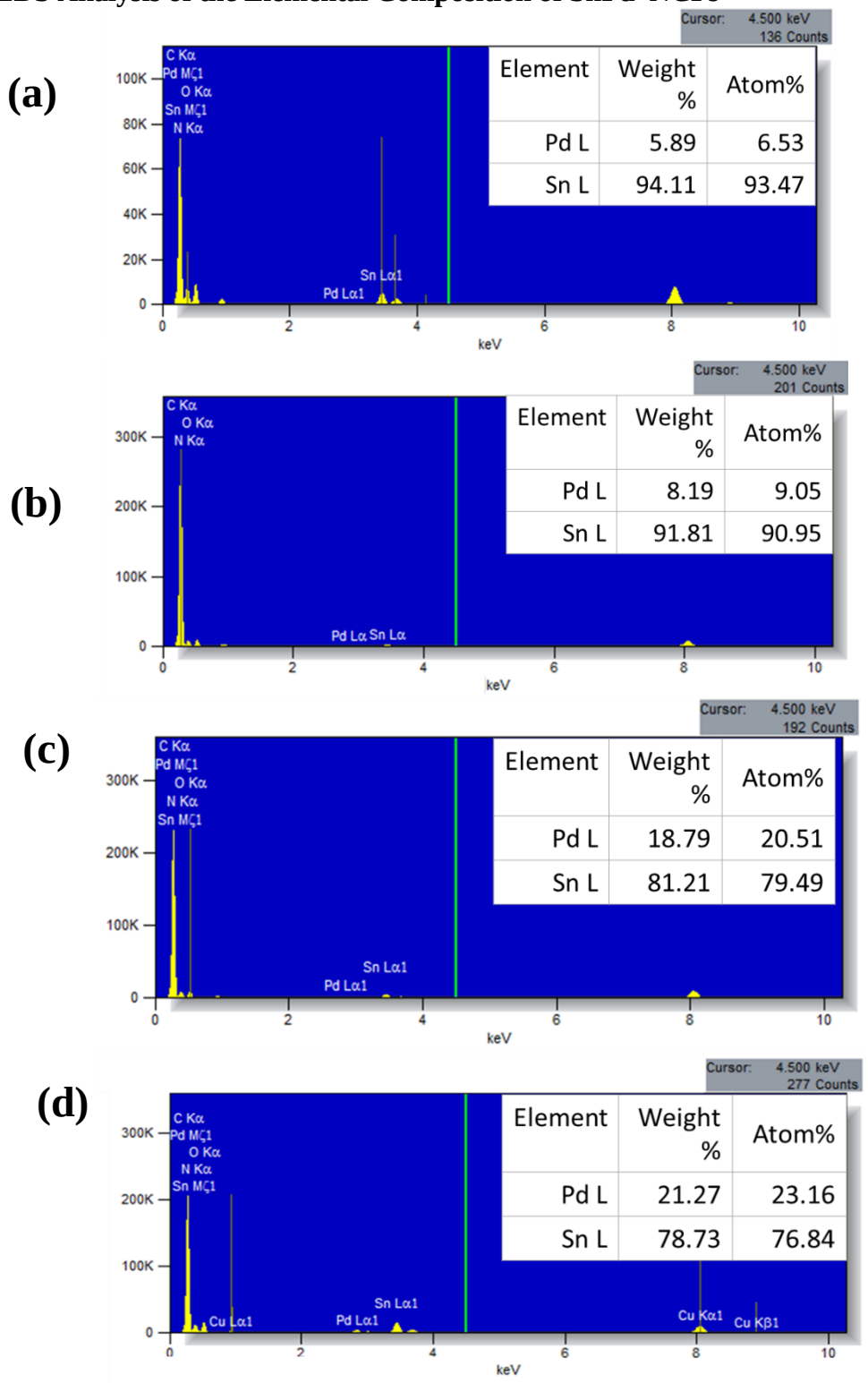

Figure S3. EDS spectra of (a) $Sn_{97}Pd_3$–NCF, (b) $Sn_{95}Pd_5$–NCF, (c) $Sn_{94}Pd_6$–NCF, and (d) $Sn_{91}Pd_9$–NCF.

S4. Ag/AgCl reference electrode calibration and conversion to RHE

We performed LSV in H_2-saturated electrolytes of 0.5 M H_2SO_4, pH 8.3 (equivalent pH of 0.5 M $KHCO_3$) and pH 7.2 (equivalent pH of CO_2-saturated 0.5 M $KHCO_3$), using a Pt wire as the working electrode and counter electrode at a scan rate of 1 mV/s to convert the $E_{Ag/AgCl}$ to E_{RHE} (Figure S4). The potential at which zero current was obtained was the thermodynamic potential equivalent RHE at that pH. The potential at which zero current was obtained was pH 0 = 0.208 V (considered as $E_{Ag/AgCl}$), pH 7.2 =0.634 V, and pH 8.3 = 0.701 V. The reported current density values were normalized to the geometric area of the electrode.

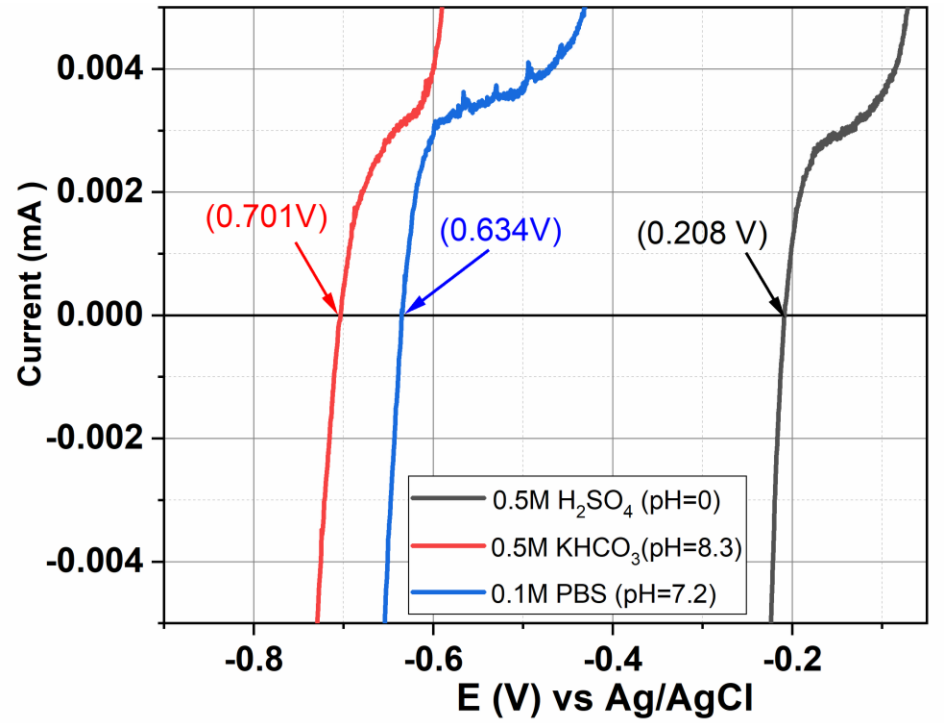

Figure S4. Linear sweep voltammograms performed using Pt as the working and counter electrodes and Ag/AgCl as a reference electrode in hydrogen-saturated 0.5 M H_2SO_4, 0.5 M $KHCO_3$, and 0.1 M PBS at pH 7.2.

S5. Linear sweep voltammetry in N_2- and CO_2-saturated 0.5 M $KHCO_3$ solutions

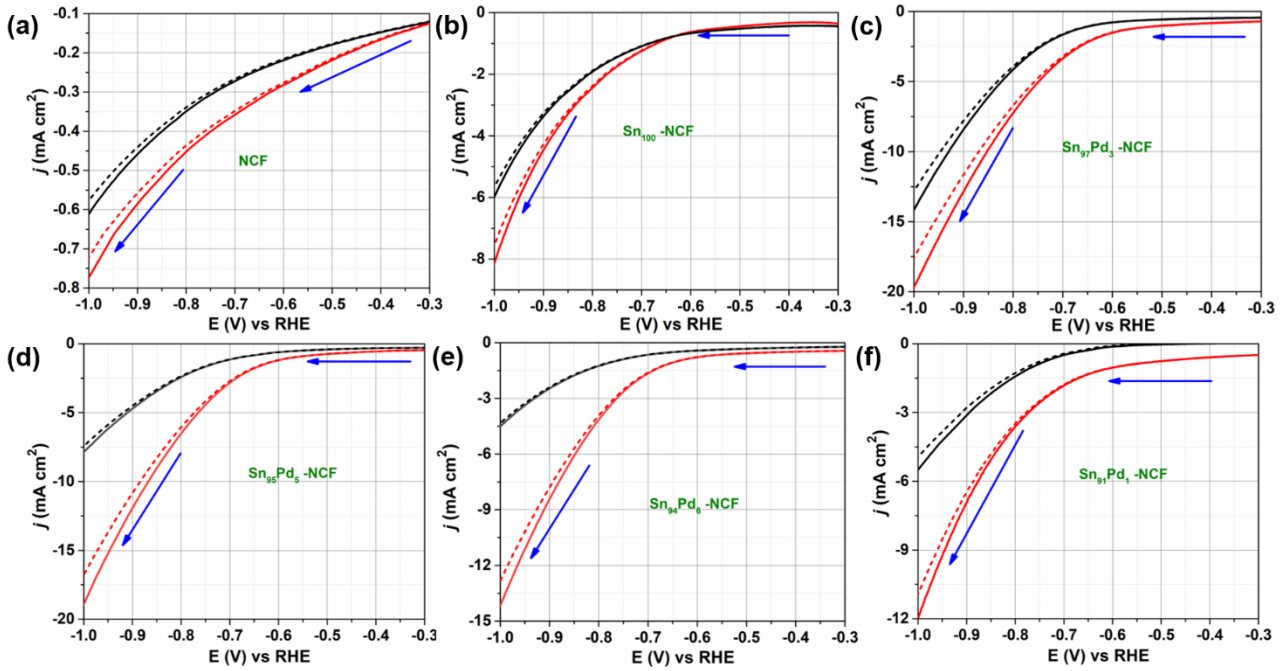

Figure S5. Linear sweep voltammograms of (a) NCF, (b) Sn_{100}–NCF, (c) $Sn_{97}Pd_3$–NCF, (d) $Sn_{95}Pd_5$–NCF, (e) $Sn_{94}Pd_6$–NCF, and (f) $Sn_{91}Pd_9$–NCF measured in N_2- and CO_2-saturated 0.5 M $KHCO_3$ solutions before (dotted lines) and after (solid lines) iR correction.

S6. Product Analysis and Faradaic efficiency.

S6.1 NMR spectra and formate calibration

An aliquot (0.5 mL) of catholyte was collected after electrolysis and mixed with 0.1 mL of D_2O and 0.1 mL DMSO (3.5 mM). The ^1H spectrum of the mixture was measured with water suppression and a presaturation method using a Bruker 400 MHz NMR spectrometer. The amount of formate produced was calculated by comparing the integral areas of the formate peak with the DMSO peak [1]. The NMR instrument was calibrated by plotting a calibration curve (Figure S6) using standard solutions of formate prepared from potassium formate (Wako Chemicals)

The Faradaic efficiency was calculated using the following equation:

$$Faradaic\ Efficiency\ for\ formate = \frac{n\,2\,F}{q} \times 100 \qquad (1)$$

where n is the number of moles of formate produced calculated from the NMR spectrum, F is the Faraday constant and q is the number of coulombs transferred.

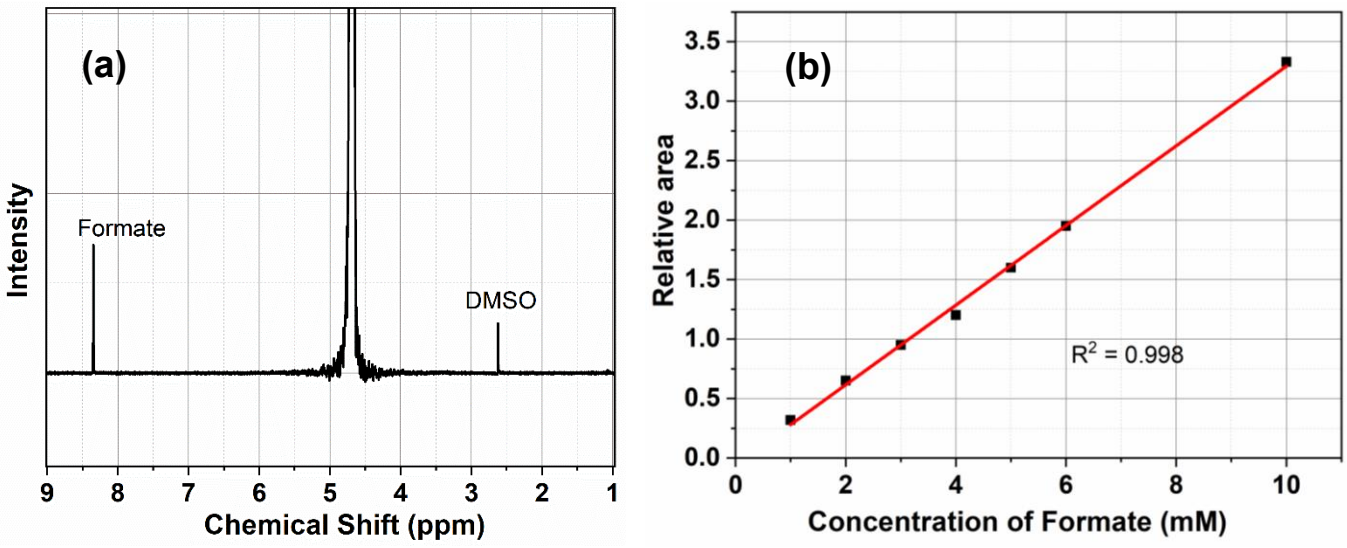

Figure S6. (a) ^{1}H NMR spectra of a 0.5 M $KHCO_3$ electrolyte containing the CO_2 reduction reaction product formate and internal standard DMSO, and (b) NMR calibration curve obtained by plotting the linear relationship between the formate concentration and relative area vs DMSO.

S6.2 Gas Chromatography

Gas products were quantified using a gas chromatograph (Shimadzu GC-2010 Tracera) equipped with Micropacked ST in series with a Shincarbon ST column and Barrier Discharge Ionization Detector (BID). Ultrahigh purity helium was used as the carrier gas. The gas products of CO_2RR along with the flowed CO_2 gas at a flow rate of 100 mL/min were measured from the cathodic compartment by directly venting them into the gas chromatograph. The Faradaic efficiency of the gas products was calculated using the following equation [2]:

$$Faradaic\ Efficiency\ of\ \frac{CO}{H_2} = \frac{peak\ area\ \times flow\ rate\ \times 2Fp_0 \times (electrode\ area)^{-1})}{\alpha \times RT \times j} \times 100 \qquad (2)$$

where α is a conversion factor based on the calibration of the gas chromatograph with standard samples (which is 72. 3 for H_2 and 992.6 for CO), p_0 =1.013 bar, F is the Faraday constant, R is the gas constant, T= 298 K and j is the total current density.

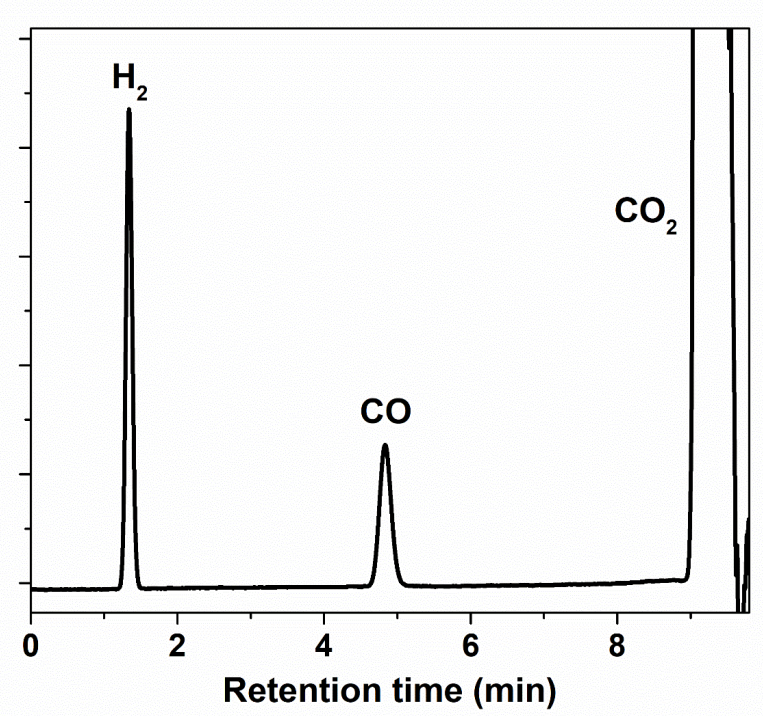

Figure S7. Representative GC spectrum of the CO_2 reduction reaction product.

S6.3 Faradaic efficiencies of NCF

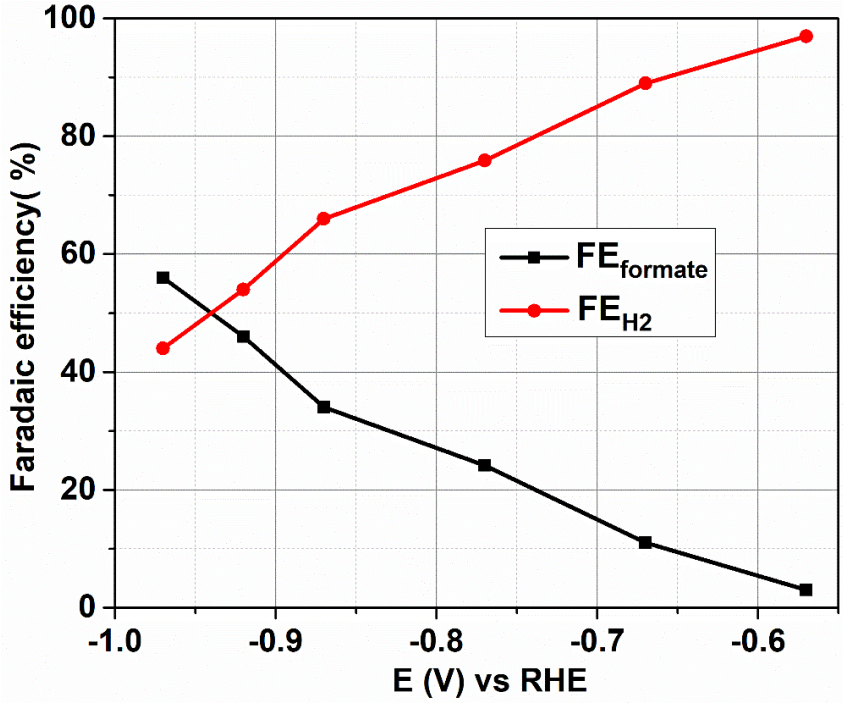

Figure S8. Formate and hydrogen faradaic efficiency of N- doped carbon fibers

S7. Partial current density and FE_{H2}

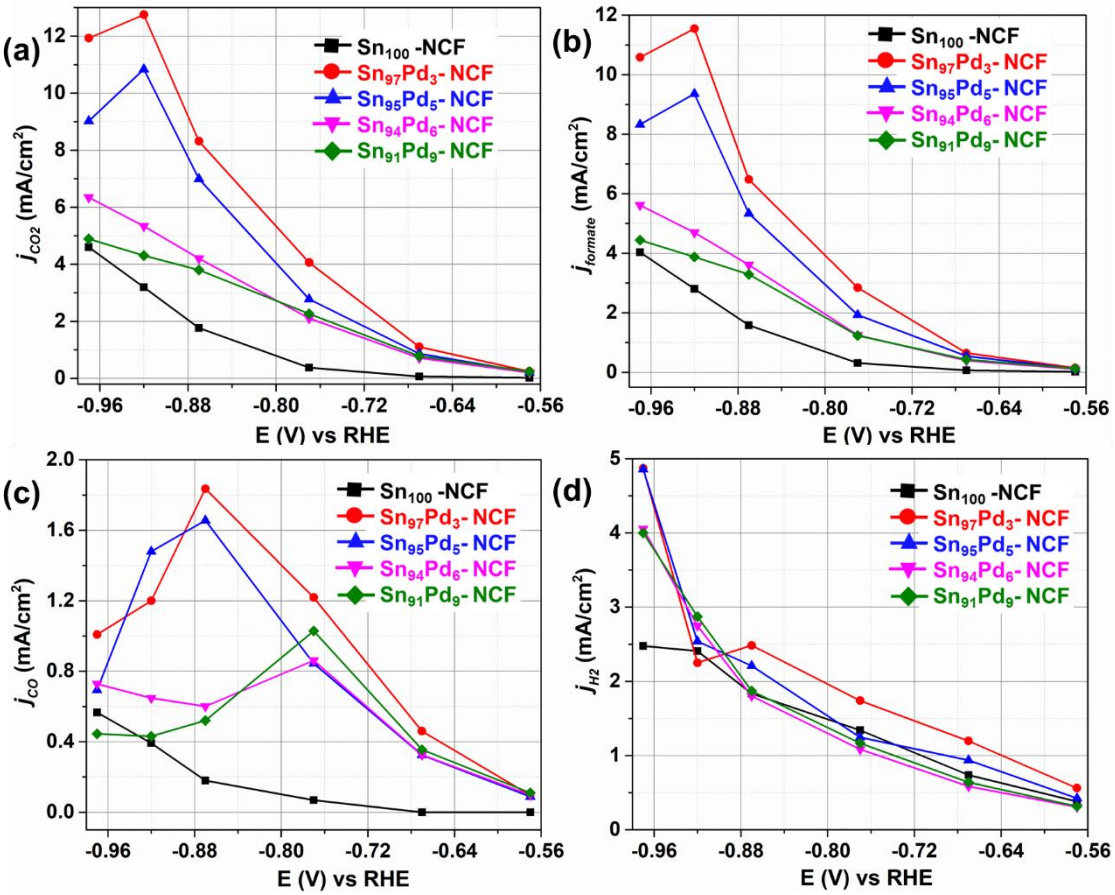

Figure S9. (a) j_{CO2}, (b) $j_{formate}$, (c) j_{CO} and (d) j_{H2} of Sn_{100}–NCF and $Sn_{100-y}Pd_y$–NCF

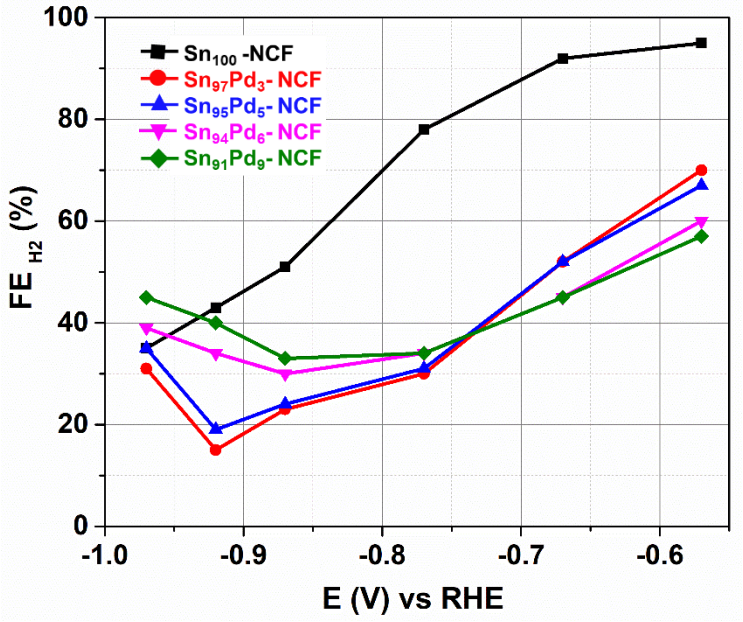

Figure S10. Hydrogen faradaic efficiency of Sn_{100}–NCF and $Sn_{100-y}Pd_y$–NCF.

S8. Electrochemical CO_2 reduction on PdO

The electrochemical CO_2 reduction activity of PdO was tested in a 0.5 M $KHCO_3$ solution saturated with CO_2. 1cm^2 and 0.5 mm thick oxidized Pd sheet was used as the electrode. Pd was oxidized by thermal treatment as reported elsewhere [3]. Constant potential electrolysis was performed by applying – 0.37 V for 30 minutes under a constant flow of CO_2. An aliquot of electrolyte was collected every 10 minutes and NMR analysis was performed for calculating the formate faradaic efficiency. XRD analysis of PdO was performed before, in between, and after electrolysis.

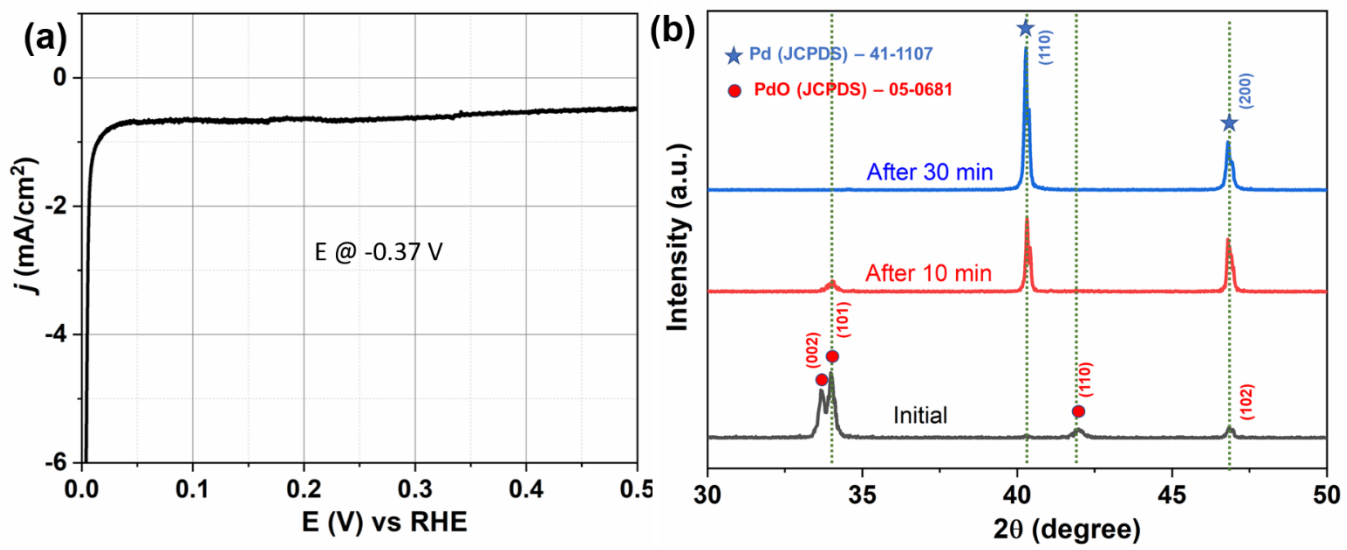

Figure S11.(a) Constant potential electrolysis of CO_2 at – 0.37 V and (a) XRD patterns of PdO at different stages of electrolysis.

S9. Stability assessment: Constant potential CO_2 electrolysis.

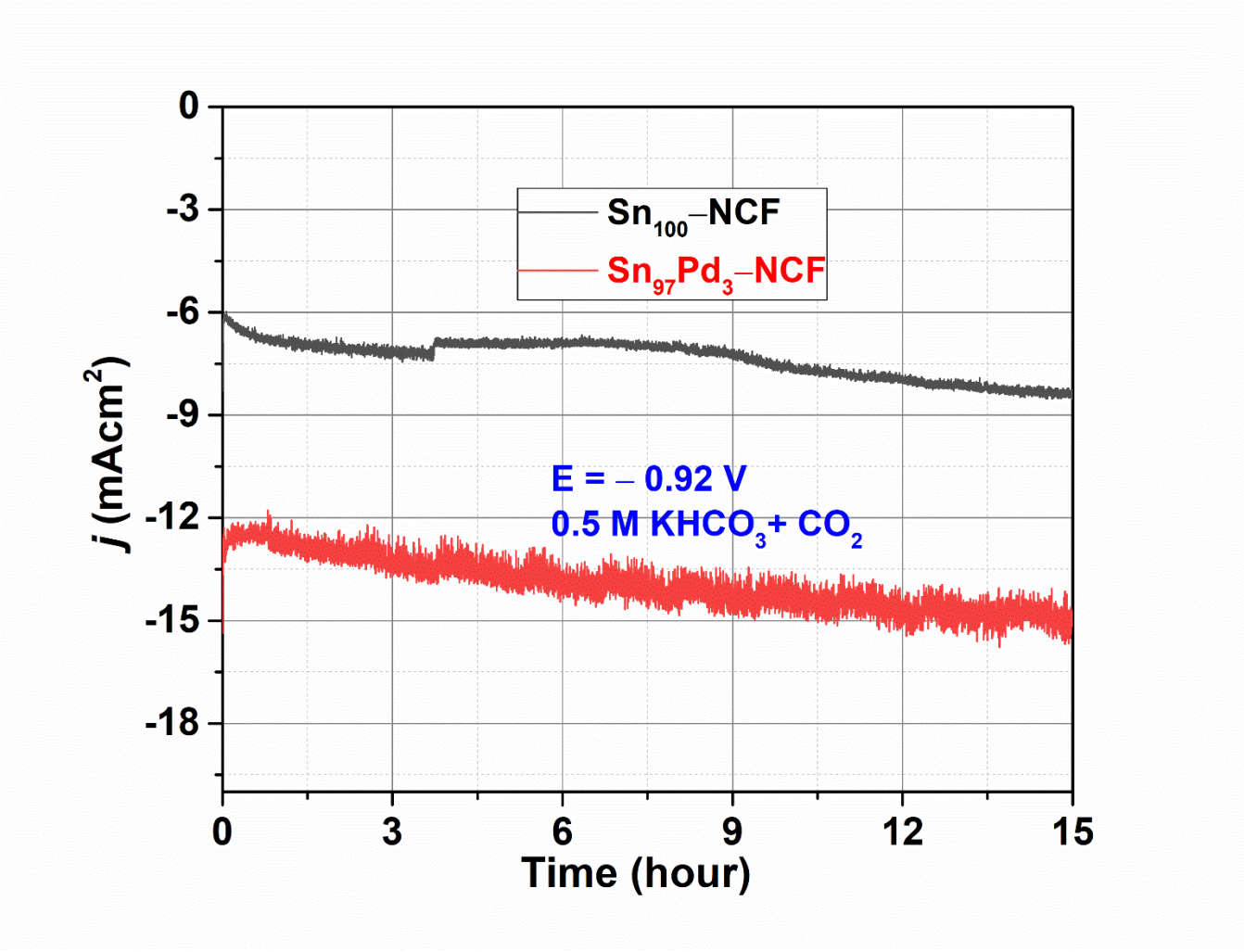

Figure S12. Constant potential electrolysis for CO_2 reduction on Sn_{100}–NCF and $Sn_{97}Pd_3$-NCF at – 0.92 V compared with the RHE in 0.5 M $KHCO_3$ saturated with CO_2.

S10. Material characterization of $Sn_{97}Pd_3$–NCF after Electrolysis

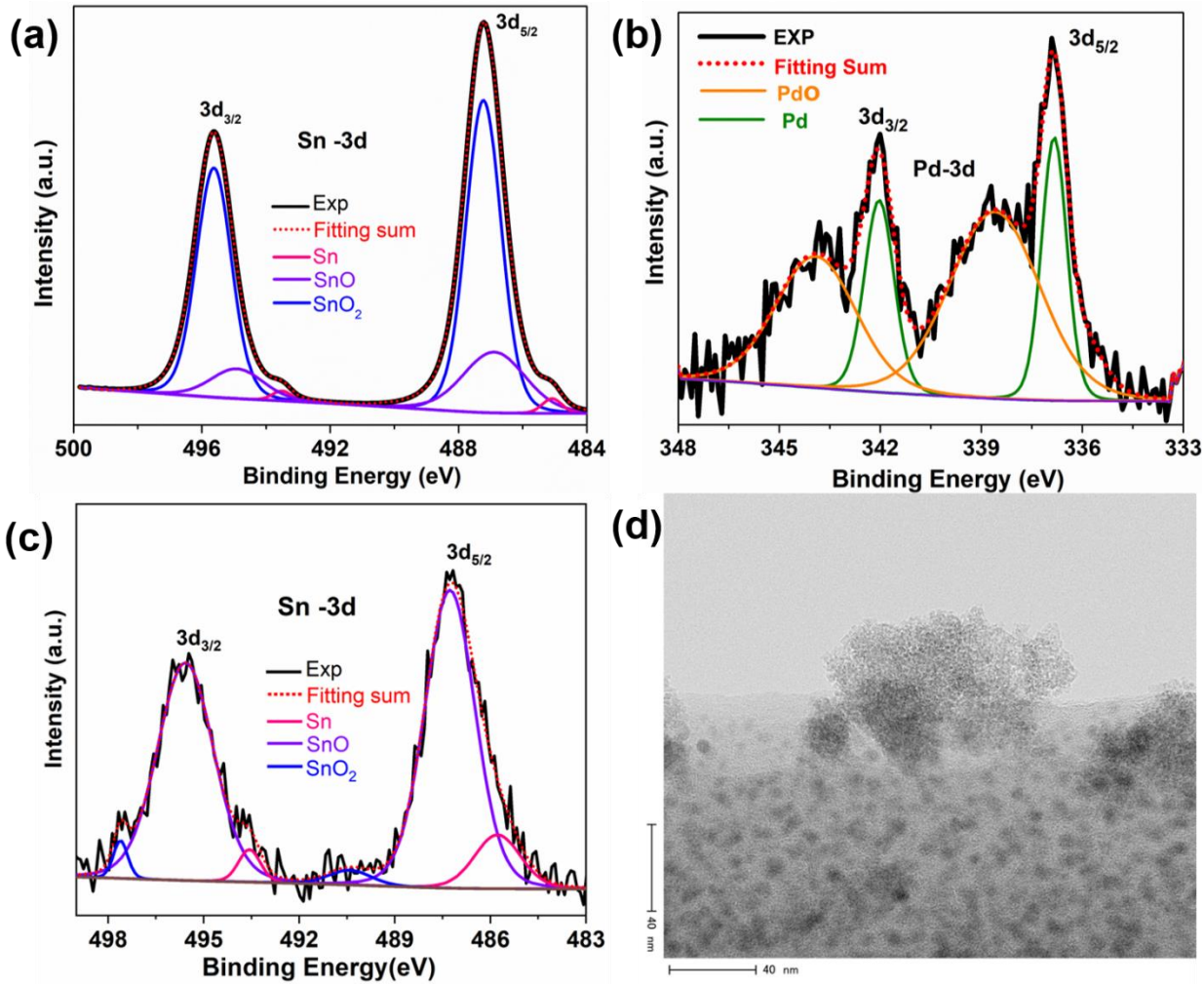

Figure S13. Deconvoluted XPS spectra of (a) Sn-3d and (b) Pd-3d after 9 hours of electrolysis, (c) Sn-3d after 15 hours of electrolysis, and (d) HR-TEM images of the $Sn_{97}Pd_3$-NCF catalyst after 15 hours electrolysis (scale bar 40 nm).

S11. Impedance Spectroscopy Analysis

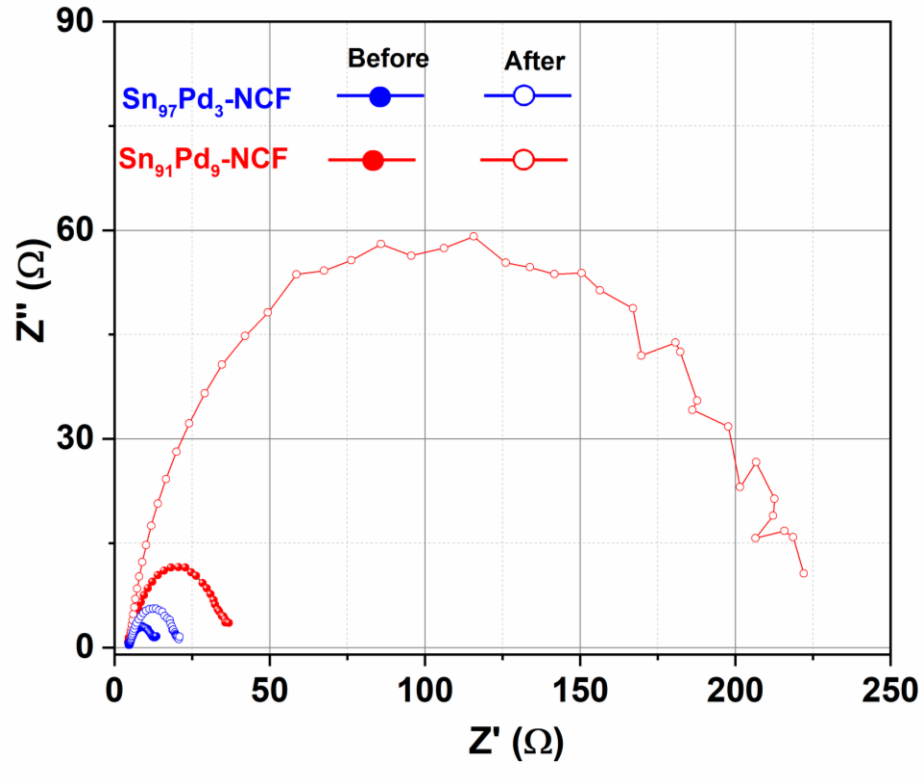

Figure S14. Nyquist plots of $Sn_{97}Pd_3$–NCF and $Sn_{91}Pd_9$–NCF measured at –0.87 V before and after CO_2 electrolysis.

Catalyst	RCT values (Ω)	
	At – 0.37 V	At – 0.87 V
$Sn_{91}Pd_9$–NCF	**33**	**30**
$Sn_{94}Pd_6$–NCF	**35**	**24**
$Sn_{95}Pd_5$–NCF	**43**	**16**
$Sn_{97}Pd_3$–NCF	**47**	**7**
Sn_{100}–NCF	**100**	**81**

Table S3. R_{CT} values of Sn_{100}–NCF and SnPd–NCF catalysts were measured in a CO_2-saturated 0.5 M $KHCO_3$ solution at –0.37 V and –0.87 V**.**

S12. Tafel plot of the Sn_{100}-NCF Catalyst

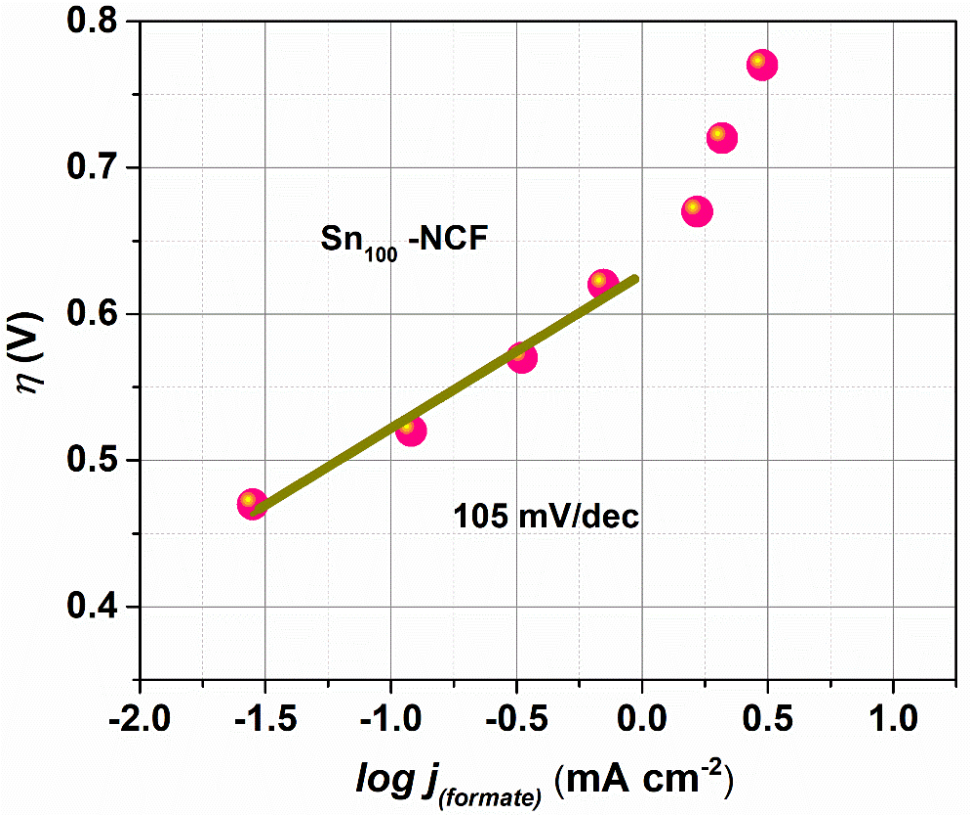

Figure S15. Tafel plot of Sn_{100}-NCF.

S13. Bicarbonate reduction on $Sn_{100-y}Pd_y$-NCF catalysts.

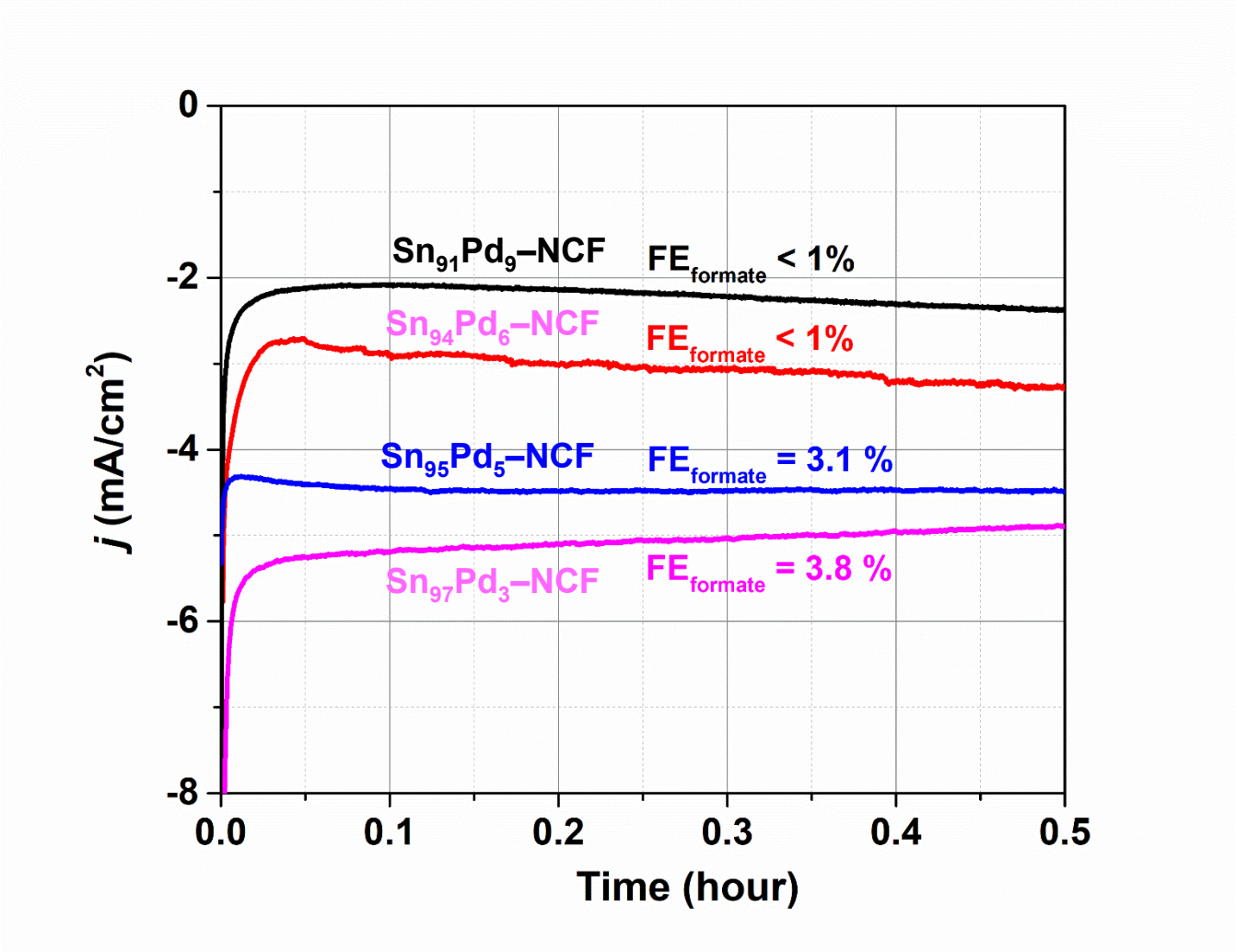

Figure S16. Constant potential electrolysis for bicarbonate reduction on $Sn_{100-y}Pd_y$-NCF in 0.5 M $KHCO_3$ saturated with N_2.

S14. Bicarbonate reduction reaction on Pd and PdO surface.

Electrochemical bicarbonate reduction activity of Pd and PdO was tested in a 0.5 M $KHCO_3$ solution saturated with N_2. 1cm^2 and 0.5 mm thick Pd and oxidized Pd sheet was used as the electrode.. Bicarbonate electrolysis was performed by applying a constant potential of – 0.50 V for one hour under a constant flow of N_2.

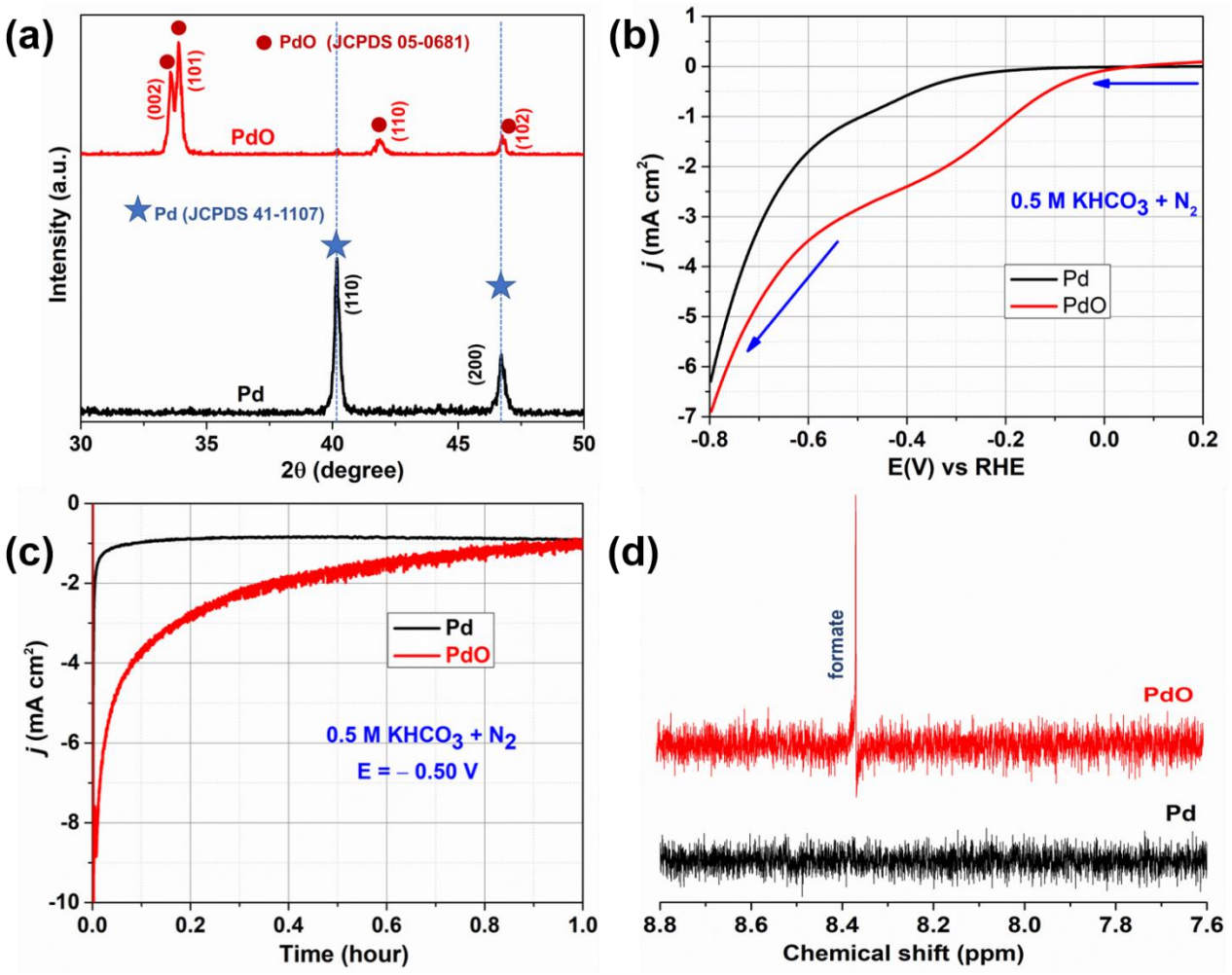

Figure S17. Material characterization and electrochemical bicarbonate reduction activity of Pd and PdO (a) XRD patterns (b) Linear sweep voltammogram measured in N_2 saturated 0.5 M $KHCO_3$ at a scan rate of 10 mV/s (c) Constant potential electrolysis at – 0.50 V, and (d) ^1H NMR spectra of bicarbonate electrolyte after electrochemical reduction reaction.

S15. Comparison of the catalytic activity of $Sn_{97}Pd_3$–NCF with other benchmarked Sn-based electrocatalysts.

Table S4. Comparison of the electrocatalytic CO_2RR activities of different Sn-based catalysts for formate production.

Catalyst	Catalyst (metal) Loading (mg/cm^2)	Electrolyte	Applied Potential (V vs RHE)	Faradaic Efficiency %	Partial current density ($mA\ cm^{-2}$)	References
$Sn_{97}Pd_3$–NCF	**0.05**	**0.5 M $KHCO_3$**	**–0.92**	**77**	**11.5**	**This study**
Sn-modified N-doped carbon fibers	0.97	0.5 M $KHCO_3$	–0.8	62	11.0	4
Sn/GDE	5.0	0.5 M $KHCO_3$	–1.17	72.9	9.8	5
PdSn/C	0.5	0.5 M $KHCO_3$	–0.46	100	2.0	6
Sn/GDE	3.0	0.5 M $NaHCO_3$	–1.1	71	5.8	7
Sn/GDE	0.7	0.5 M $NaHCO_3$	–1.17	70	18.9	8
Porous SnO_2/carbon cloth	1.02	0.5 M $NaHCO_3$	–0.92	89	43.0	9
Sn-pNWs	4.0	0.1 M $KHCO_3$	–0.8	80	4.8	10
m-SnO_2	1.0	0.1 M $KHCO_3$	–1.15	75	8.2	11
Sn/GDE	2.0	0.1 M $KHCO_3$	–1.2	64.1	2	12
SnO_2/graphene	0.21	0.1 M $NaHCO_3$	–1.17	93.6	9.5	13
Mn-doped SnO_2	1	0.1M KHCO3	-1.03	85	21.2	14
Thin-layered SnSe2	-	0.1 M KHCO3	–0.8	91 ± 4	15.2	15
Nanorod@sheet SnO	1	1 M KOH	−0.7	94	−330	16

References

1. K. P. Kuhl, E. R. Cave, D. N. Abram, and T. F. Jaramillo, *Energy Environ. Sci.*, 2012, 5, 7050–7059.

2. Y. Chen, C. W. Li, and M. W. Kanan, *J. Am. Chem. Soc.*, 2012, 134, 19969–19972.

3. W. T. Grubb and L. H. King, *Anal. Chem*., 1980, 52, 270-273.

4. Y. Zhao, J. Liang, C. Wang, J. Ma, and G. G. Wallace, *Adv. Energy Mater*., 2018, 8, 1–9.

5. Q. Wang, H. Dong and H. Yu, *RSC Adv.*, 2014, 4, 59970–59976.

6. X. Bai, W. Chen, C. Zhao, S. Li, Y. Song, R. Ge, W. Wei and Y. Sun, *Angew. Chemie - Int. Ed.*, 2017, 56, 12219–12223.

7. E. Irtem, T. Andreu, A. Parra, M. D. Hernández-Alonso, S. García-Rodríguez, J. M. Riesco-García, G. Penelas-Pérez and J. R. Morante, *J. Mater. Chem. A*, 2016, 4, 13582.

8. G. K. S Prakash, F. A.Viva, and G. A.Olah, *J. Power Sources* 2013, 223,68.

9. F. Li, L. Chen, G. P. Knowles, D. R. MacFarlane, and J. Zhang, *Angew. Chemie - Int. Ed.*, 2017, 56, 505–509.

10. B. Kumar, V. Atla, J. P. Brian, S. Kumari, T. Q. Nguyen, M. Sunkara, and J. M. Spurgeon, *Angew. Chemie - Int. Ed.*, 2017, 56, 3645–3649.

11. R. Daiyan, X. Lu, W. H. Saputera, Y. H. Ng and R. Amal, *ACS Sustain. Chem. Eng.*, 2018, 6, 1670–1679.

12. S. Zhang, P. Kang, and T. J. Meyer, *J. Am. Chem. Soc.*, 2014, 136, 1734–1737.

13. J. Wu, F. G. Risalvato, S.Ma, and X. D. Zhou, *J. Mater. Chem. A*, 2014, ***2***, 1647–1651.

14. Y.Wei, J. Liu, F. Cheng and Jun Chen, J. Mater. Chem. A, 2019, 7, 19651–19656

15. H.Yang, H. Liu, X. Liu, Z. Zhao and J. Luo, *Catal. Sci. Technol.*, 2018, 8, 5428-5433

16. Y. Qian, Y. Liu, H. Tang, B. Lin, J. CO2 Util., 2020, 42,101287